Shock Waves in Complex Binary Solids: Cubic Laves Crystals, Quasicrystals, and Amorphous Solids

Johannes Roth
Institut für Theoretische und Angewandte Physik,
Universität Stuttgart, Pfaffenwaldring 57, 70550 Stuttgart, Germany
(Dated: November 22, 2004)

Shock waves have been simulated by molecular dynamics in the cubic Laves phase C15, in related Frank-Kasper-type (AlCu)Li quasicrystals, and in an amorphous solid of the same composition and potential parameters. The goal of this study was to generate shock waves in periodic and aperiodic structures and to compare their behavior. The expectation was that new types of defects would show up in aperiodic materials. Three regimes are observed in the Laves phase: at low shock wave intensity the system reacts elastically, at high intensities it turns disordered. In the intermediate region the velocity of the elastic wave saturates and an additional plastic wave appears. Extended defects are created which form a network of walls of finite width. The crystallites in between are rotated by the shock wave. If the samples are quenched a polycrystalline phase is obtained. The size of the grains decreases with increasing shock wave intensity until complete fragmentation occurs in the third regime. The behavior of the quasicrystal models is similar, except that there is a continuous transition from a quasi-elastic behavior to the plastic regime. Ring processes are observed which break up into open paths when the shock wave energy grows. The transition to a complete destruction of the structure is continuous. In the amorphous solid a linear $u_s - u_p$-relation is found over the whole range of piston velocities. Two regimes are present, with unsteady plastic waves at weak shock strengths and steady waves in the range coinciding with the upper regime in the ordered structures.

PACS numbers: 62.50.+p, 61.44.Br, 02.70.Ns
Keywords: quasicrystals, shock waves, molecular dynamics simulations

I. INTRODUCTION

Shock wave experiments and simulations are valuable tools to expose a solid to strong uniaxial stress and to introduce defects without explicitly constructing them. Defects generated by shock waves have been studied in monatomic crystals to some depth[1–4]. The shock stress relaxes to an energetically more favorable hydrodynamically compressed state for example by slippage or phase transformations. Often stacking faults are created which permit a direct detection of the slippage.

For an ordinary crystal structure it is rather easy to construct slip planes and stacking faults and to analyze them. This is not the case for quasicrystals. If geometric constructions are used, complicated and rather arbitrary procedures have to be carried out to create for example dislocations and associated extended defects. These problems may be avoided if shock waves are studied: Now the structure itself selects the defect planes and the Burgers vectors. A drawback may be that most often high-energy defect structures are created, which may not be representative for slow deformations and low-energy plasticity.

The first goal of the present study was to find out whether quasicrystals behave different than other materials if they are penetrated by shock waves. Many real metals and alloys as well as fcc model crystals with Lennard-Jones interactions, if shocked along the $\langle 100 \rangle$ direction[1], show a rather universal behavior with respect to the shock front velocity. The same is true for quasicrystals, binary crystals and binary amorphous solids in the case of strong shock waves. For weak shock waves a deviation is observed due to elastic precursor effects. A similar deviation has been found recently for fcc crystals[1] along the $\langle 110 \rangle$ and the $\langle 111 \rangle$ directions.

The second goal was to find out if new kinds of defects occur in the quasicrystal. According to Holian[5], a real shock wave in a crystal (as opposed to a very strong elastic wave) causes permanent plastic deformations, but with respect to stability the supersonic elastic waves are also shock waves. Often stacking faults are observed which are the trace of the slippage. Twinning and martensitic deformations are also very common. In quasicrystals all these defects are also allowed but additional types of defects are possible: flips, where a few atoms change to alternative sites, phason walls, where after slippage the aperiodic sequence of lattice planes does not fit anymore, or transformations to crystals and approximants. It turns out that in the models studied here the defects which show up in the quasicrystals are indeed different from those expected for monatomic crystals but that they are similar to those in the closely related binary Laves crystal. Weak shock waves merely cause elastic distortion whereas strong shock waves destroy the structure completely. Therefore they both will not be studied in detail. We will concentrate on the defect structures generated in the intermediate range.

The relation between the shock wave velocity u_s and the piston velocity u_p is studied in detail for shock waves along all major symmetry directions. The question of steadiness of the wave profiles will be discussed. The defects accompanying the transition from elastic to plastic

behavior will be described for the 4-fold crystalline and the 2-fold icosahedral direction. Further results have already been published elsewhere[6–8].

The influence of the ordered structure on the effect of shock waves is addressed in a further study, where shock waves in an amorphous material with the same composition have been simulated. In contrast to the crystal and the quasicrystal the Hugoniot curve is almost perfectly linear, but there are also steady and unsteady waves.

The paper is organized as follows: We will start with the simulation setup and the structure model. Next we will present the results: first the velocities of the shock waves, then the description of the defects generated, separately for the Laves crystals and the quasicrystals. The simulations of the amorphous structures follow. The last section contains the discussion of the results.

II. MODELS, INTERACTIONS, MOLECULAR DYNAMICS

A. The Structure Models

We start with the most simple structure models and expand them step by step. All structures, crystals and quasicrystals, belong to the close-packed Frank-Kasper-type, which means that a Delauney decomposition yields a space-filling of non-regular tetrahedra only.

Starting point is the C15 Laves phase. It is a periodic arrangement of prolate rhombohedra (Fig. 1, right). The rhombohedra are decorated with small atoms (light gray) at the corners and the mid-edge centers and with two large atoms (dark gray) along the body diagonal dividing it in the ratio 3:2:3. To obey the cubic symmetry the rhombohedra are slightly distorted with respect to the ones in the quasicrystal. The large atoms generate a diamond structure, the small atoms form a corner-connected network of regular tetrahedra. The edges of the rhombohedra are two-fold $\langle 110 \rangle$ axes, the long body diagonal is a three-fold $\langle 111 \rangle$ axis. The short body diagonals form the $\langle 100 \rangle$ direction which are no true four-fold axes since the crystal symmetry is Fd3m.

The next step is the TI-model[?] . It is a quasiperiodic arrangement of prolate and oblate rhombohedra (Fig. 1) on the standard three-dimensional rhombohedron tiling[9]. The prolate rhombohedron is decorated as before, but the large atoms now subdivide the body diagonal in the ratio τ:1:τ, with τ the golden mean $(1 + \sqrt{5})/2$. The oblate rhombohedron contains only small atoms at the corners and mid-edge centers[10]. In the quasicrystal models the edges point along five-fold axes, the face diagonals of the cells are two-fold axes, and the long body diagonal is a three-fold axis. Thus the orientation is different from the Laves phase!

The third step is the BI-model[?] . It has been created since the TI-model has two drawbacks: the oblate rhombohedra form under-dense and therefore unstable regions, and the stoichiometry is wrong if real quasicrystals are to be described. Therefore Henley and Elser[11] modified the TI-model by replacing compounds of two oblate and two prolate rhombohedra wherever possible with a rhombic dodecahedron (Fig.2). The outer hull of the compound and the dodecahedron are identical, but in the interior four large and five small atoms are replaced by usually eight large atoms which are placed at the corners of a hexagonal bipyramid. Depending on the quasicrystal modeled ((AlCu)Li or (AlZn)Mg) the apex sites (large light gray atoms in Fig. 2) may occupied by large or small atoms. In the case considered here they are large atoms.

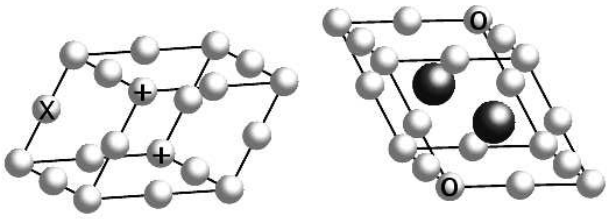

FIG. 1: Oblate and prolate rhombohedron. Light gray: small atoms, dark gray: large atoms. Left: the x marks the atom around which 10 oblate rhombohedra fit together. The atoms marked with the + form a puckered decagon, around which the ring processes occur. Right: the atoms marked with o denote the intersection points of the $\langle 100 \rangle$ direction.

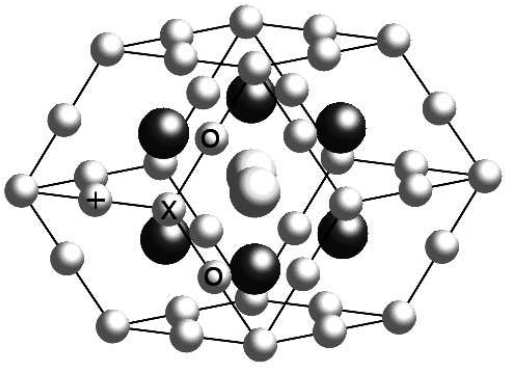

FIG. 2: The rhombic dodecahedron. The atom marked with an x and its symmetry-equivalent copies are the primary sites of flips. The large light gray atoms are also very mobile. The atoms marked with + and o are secondary sites for diffusion.

The fourth model is an amorphous solid which was generated from the Laves crystal by melting, equilibrating, quenching, and decompression to ambient pressure.

The four structures have a similar composition: The crystal and the amorphous solid carry the structure formula A_2B, the composition of the TI quasicrystal is $A_{0.764}B_{0.236}$, and the composition of the BI quasicrystal is $A_{0.629}B_{0.371}$.

Quasicrystals permit localized rearrangements of atoms, similar to diffusion processes, which may also lead to a rearrangement of the tiles. Atom jumps occur in

the TI model in equilibrium simulations already[12], and they play a major role in the shock simulations. Therefore they will be described here in some detail. Starting point are the oblate rhombohedra. If ten copies of these cells are put together at the edge marked with an x in Fig. 1, then the atoms marked with the + form a puckered decagon. The analysis of the local potential shows that the atoms can move almost freely around the decagon. This motion will be called a ring process. It is possible to replace pairs of oblate rhombohedra by one prolate rhombohedron. Then the ring is broken into parts and we speak of chains. The free motion of the atoms along a chain is hindered to a large degree, but is not completely impossible. If the TI structure is transformed into the BI structure, all rings and most of the chains are replaced by dodecahedra, and the ring processes are suppressed entirely. There are, however, a few single oblate rhombohedra, and the atoms marked with the x in Fig. 1 can still exchange their places. This leads to the flip processes in the BI-model. Other possibilities exist around the dodecahedra. The atoms marked with the x in Fig. 2 are the remains of the oblate rhombohedra, furthermore, the large atoms marked light gray have a lot of free space around them. Thus exchange processes of the large light gray atoms and the atoms marked with the x occur. A few jumps to the atoms marked with o and + have also been observed.

B. The Interaction

The interactions were modeled by Lennard-Jones potentials for two reasons: first of all, there are currently no specific potentials available for quasicrystals of the Frank-Kasper-type. Secondly, we are not interested in the first place in the behavior of a specific material but in the general damage caused by shock waves. It may be argued that the Lennard-Jones potential is not well suited for alloys, but we will comment on this objection later in the discussion. The radii of the potential minima have been adjusted to the average of the shortest AA, AB and BB distances. Such distances will be called bonds. The potential parameters are $r_{AA} = 1.0542a$, $r_{AB} = 1.23034a$, and $r_{BB} = 1.20395a$, where $a^?$ is half the edge length of the tiles. The cut-off radius for the potential was $r_C = 3.07476a = 2.5r_{AB}$. The depth of the potentials interacting between atoms of the same type is $-\epsilon$, and -2ϵ for atoms of different types. Since the potential parameters have been optimized for the TI-model, the coordinates of the Laves phase had to be rescale by 1.027 and of the BI-model by 1.0064 to obtain uncompressed initial states. With these potentials, the binding energy is 11.478ϵ for the TI quasicrystal, 12.478ϵ for the BI quasicrystal, 12.974ϵ for the Laves crystal, and 10.564ϵ for the amorphous solid.

C. Generation of Shock Waves

There are a number of well established methods to generate shock waves in simulations[13]. In the present work we use the following setup: The sample is cut into two blocks of equal size. In the simulation the two parts are moved towards each other at constant velocities $\pm u_p$. Two shock waves are created at the central plane where the blocks collide and propagate through the compound sample at velocities $\pm(u_s - u_p)$. The setup is equivalent to a piston compressing a sample at rest at speed u_p, thereby creating a shock wave at speed u_s. Test runs have shown that the momentum mirror method yields equivalent macroscopic results. The shock wave velocities for example are identical. The microscopic structure of the defects may be different, however, since the mirror enforces symmetric or antisymmetric behavior.

D. Molecular Dynamics and Preparation of the Samples

All simulations have been carried out with the IMD simulation program[14]. For the shock simulations an NVE ensemble was used. Equilibrations were performed with the NVT Nose-Hoover and NPT Andersen ensemble, depending on the the volume or pressure to be fixed. At low temperature and low pressure the differences between NVT and NPT equilibration are marginal. For the quenching of the shocked samples IMD provides the micro-convergence (mic) and the global convergence (gloc) method. The first method works in physical space separately for every particle: If the velocity $\mathbf{v}_i$ of particle i and the force $\mathbf{F}_i$ acting on it point in opposite directions, i.e. $\mathbf{F}_i \cdot \mathbf{v}_i < 0$, then the velocity $\mathbf{v}_i$ is set to 0. In the second case the system as a whole is examined in $3N$-dimensional configuration space: If the velocity vector $\vec{v} = \{\mathbf{v}_1, \mathbf{v}_2, \ldots, \mathbf{v}_N\}$ and the force $\vec{f} = \{\mathbf{F}_1, \mathbf{F}_2, \ldots, \mathbf{F}_N\}$ point in opposite directions, i.e. $\vec{f} \cdot \vec{v} = \sum_{i=1}^{N} \mathbf{F}_i \cdot \mathbf{v}_i < 0$, then the velocities $\mathbf{v}_i$ of all particles are set to zero. If a sample is close to equilibrium, the gloc method works much better than mic, especially if one tries to remove the kinetic energy. For the shocked structures, however, it was necessary to reduce the energy with the mic method first and then to minimize it with the gloc method.

The sample sizes ranged from 20,000 up to about a million atoms for both crystals and quasicrystals. The samples are long rods with cross-sections between 14×14 to $61 \times 61a^2$ and lengths between 100 and $260a$. The boundaries were open along the shock wave propagation direction and periodic along the two transverse directions. For the amorphous solid we used samples with 80,000 atoms and size $160 \times 14 \times 14a^3$. To enable periodic boundary conditions the perfect icosahedral quasicrystal is replaced by an orthorhombic approximant.

After the samples were generated they are equilibrated for a time interval of $t = 10t_0$ at $kT = 0.001\epsilon$ and pressure

$P = 0.01P_0$. When the shock waves have passed through the samples they are quenched to $T = 0$ to remove the random displacements of the atoms caused by the heating and deformation.

III. RESULTS

A. Elasticity and Anisotropy of the Sound Waves

In linear elasticity icosahedral quasicrystals behave elastically isotropic whereas the cubic Laves crystal are anisotropic. We have computed the elastic constants for a number of directions by quasi-static uniaxial deformation of the samples. The (quasi)-longitudinal velocity of sound is then given by $c_l = \sqrt{F/\rho}$ where F is the elastic constant for uniaxial deformation and ρ is the density. For the Laves crystal indeed a strong anisotropy is found (The indices are the lattice directions): $c_{l\langle 100\rangle} = 14.29v_0$, $c_{l\langle 111\rangle} = 12.81v_0$, $c_{l\langle 110\rangle} = 13.20v_0$. The relation $4c_{l\langle 110\rangle} - 3c_{l\langle 111\rangle} = c_{l\langle 100\rangle}$ for cubic crystals is fulfilled. For the TI quasicrystal the velocities of sound along the major symmetry directions are $c_{l2} = 12.22v_0$, $c_{l3} = 12.29v_0$, $c_{l5} = 12.21v_0$. For the BI quasicrystal they are $c_{l2} = 9.88v_0$, $c_{l3} = 10.00v_0$, $c_{l5} = 9.95v_0$. The velocity of sound of the amorphous solid is $c_0 \approx 10v_0$. If all directions are taken into account an anisotropy of about 2% is found for the Laves crystal while only 0.2% are calculated for the TI quasicrystal and 0.8% for the BI quasicrystal. An explanation for the larger anisotropy of the BI samples may be that their icosahedral "quality" is worse since the modification of the structure is more severe.

In the elastic shock wave regime the relation $u_s = au_p + b$ holds between the velocity of the shock wave u_s and the piston velocity u_p. If the strength of the shock wave goes to zero, the velocity u_s should be the velocity of an elastic sound wave. The constants b derived accordingly are indeed close to the velocities of sound c_l obtained from the quasi-static computations for all directions that have been studied in the simulations.

B. Pressure Profiles and Steadiness of the Profiles

1. Nature of the Wave Fronts

The behavior of the samples with increasing shock strength can be subdivided into three regimes with respect to the observed wave fronts. The criterion is the steadiness of the wave profiles. A wave front is called steady if it does not change its shape in time. It frequently happens that a wave profile is not steady as a whole but contains steady parts, for example a steady elastic and plastic front separated by a spreading and therefore unsteady plastic precursor[15]. In this case the steadiness of each part will be addressed separately.

Here we will shortly sketch the three different regimes occurring in the simulations. Details about the pressure profiles and the u_s-u_p-relation follow in the next sections.

In the simulations presented here, a single steady elastic wave front is observed below $u_s/c_l \leq 0.3$. Between $u_s/c_l = 0.3$ and 0.6, a two wave structure is found. More precisely, the previous elastic front is turned into an elastic precursor which reaches a steady state during simulation, followed by a continuously spreading plastic precursor. A steady plastic front is not present. Above $u_s/c_l = 0.6$, steady waves are occurring. A steady elastic wave front is immediately followed by a steady plastic front moving at the same speed. With increasing shock strength, the elastic precursor in the second regime develops continuously into the steady plastic front in the third regime by steepening of the profile.

Although the plastic profiles in the second regime are non-steady, the structure itself reaches a steady state at the center where the shock waves started. This means that the uniaxial pressure and the shear stress converge to a finite value and the structure relaxes.

2. Pressure Profiles

During simulation, the distributions of the instantaneous pressures averaged over the cross section of the samples are computed as a function of the propagation direction x and time. From the uniaxial components P_{xx}, P_{yy}, and P_{zz} the hydrostatic pressure $P = (P_{xx} + P_{yy} + P_{zz})/3$ and the shear pressure $S = P_{xx} - (P_{yy} + P_{zz})/2$ can be derived. In the following we will concentrate on the uniaxial pressure P_{xx} and the shear pressure S. The shape of the pressure profiles as a function of the piston velocity u_p fits exactly into the three regime picture set up in Sec. III B 1. The results are as a rule identical for all samples and all directions, therefore they will be presented summarily. Differences will be pointed out where appropriate.

In the first elastic regime P_{xx} and S rise sharply at the shock front and stay constant along the sample (Fig. 3 and 4, Laves crystal). The samples are compressed uniaxially, and no plasticity is observed. In the Laves crystals up to four oscillations with an amplitude of half the plateau value and a wavelength of about $7a$ are found. They are not present in the quasicrystal and are similar to the locked-in solitary waves described for example by Germann et al.[1]

In the second regime where defects are created, the wave profile as a whole *does not* become steady during simulation (Fig. 3 and 4, TI quasicrystal at $u_p/c_l = 0.37$). The shear pressure S rises sharply, but then it decays continuously the whole way down to the center of the sample. The uniaxial and the shear pressure at the center of the sample drop during simulation, indicating a relaxation of the structure. But if u_s/c_l is larger than about 0.25 for the TI model and 0.4 for the Laves crystal, a constant value is reached after some time, indicat-

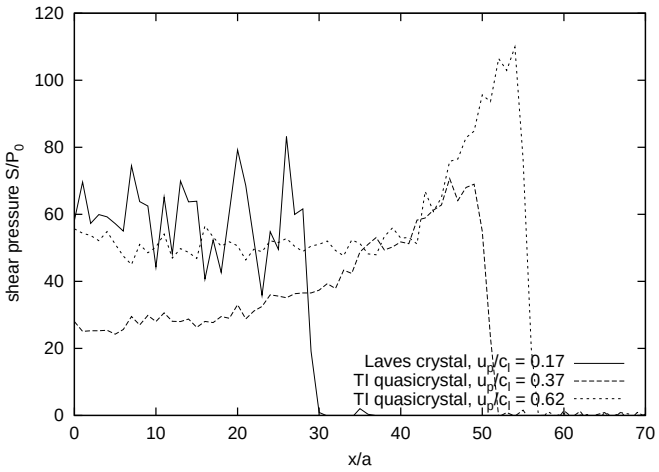

FIG. 3: Shear pressure S of three samples representative for the three regimes.

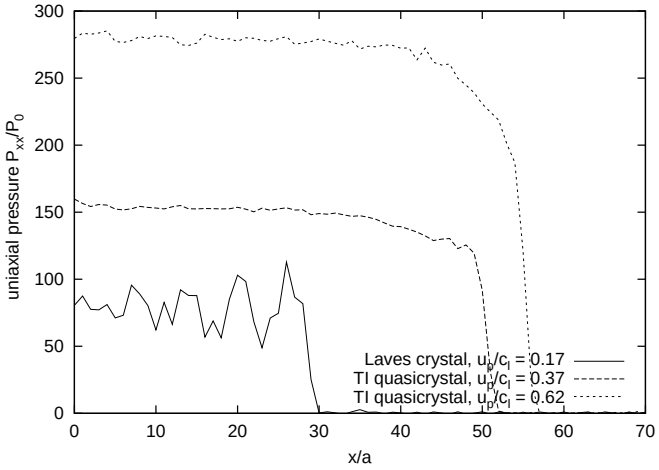

FIG. 4: Uniaxial pressure P_{xx} of three samples typical for the three regimes.

ing that the structure has reached a relaxed state. There is a remarkable difference between the quasicrystal models and the Laves crystal: In the quasicrystal S falls of directly behind the shock front whereas in the Laves crystal a plateau exists which proves that the elastically compressed sample breaks and plasticity sets in with delay. The uniaxial pressure P_{xx} behaves complementary: Instead of the sharp rise and slow decay it grows slowly until it reaches a plateau at the location where S has dropped to about the half of its peak value. If u_p is larger than 0.45 in the case of the Laves crystal, the convergence of P_{xx} and S to a constant plateau can already be anticipated. In the Laves crystal the oscillations of the profile in the elastically compressed part of the sample as described in the first regime are still observable.

In the third regime the curve of the shear pressure S resembles the shape in the second regime at a first glance, but now the profile is clearly steady (Fig. 3 and 4, TI quasicrystal at $u_p/c_l = 0.62$). The shear pressure first rises sharply at the shock front, but then it drops within a fixed interval of 10 to $15a$ to its final plateau value. The uniaxial pressure P_{xx} grows slowly within the same range. Hence the plastic destruction sets in after only a very short elastic reaction.

In a liquid the shear pressure S should drop to zero after shock compression since there is no shear elasticity and the liquid can flow freely. Such a behavior is certainly not found in our simulations, neither in the second, nor in the third regime. The shear pressure is a monotonously rising function of the piston velocity u_p with changing slopes in the three regimes. It is expected that S will drop due to relaxation processes. But they are too slow to be observed on the simulation time scale.

C. The Hugoniot Relation u_s-u_p in General

In a u_s-u_p-Hugoniot plot the velocities u_s of the elastic and plastic wave fronts are drawn vs. the piston velocity u_p. The velocities u_s were determined in two ways: either from the slope of the wave fronts in time-distance contour plots, or directly from histograms of the uniaxial or shear pressure with time as a parameter. Two factors limit to the accuracy: Often there are large fluctuations of the pressures, and sometimes slow relaxation phenomena occur leading to decreasing wave velocities and changing pressures. The fluctuations are caused by the discrete nature of the sample which leads to a strong variation of the number of particles in the histogram bins. This problem is even more severe in the case of the aperiodic, but well ordered quasicrystals. The fluctuations can be avoided to some degree by averaging in a comoving frame, but only if the wave profile is steady. The relaxation phenomena themselves can only be avoided by much longer simulation times which also require much larger samples beyond our current computing capacities. It must be stressed, however, that larger simulations are not expected to lead to qualitatively new results since relaxed states can be obtained at the center of the samples if the shock strength is not too small.

In Fig. 5 we present the typical form of a u_s-u_p-Hugoniot plot for shock waves in the Laves crystals along the four-fold direction and in the TI quasicrystals along the two-fold direction, respectively. The BI quasicrystals show similar behavior. The curves are characteristic for a material which reacts elastically below a certain threshold. Then delayed plastic deformation sets in until at high shock intensities the structure is destroyed directly behind the shock front.

At low piston velocities elastic shock waves and a material-dependent gradient are observed. The slopes $(u_s - c_l)/u_p$ are 3.1 for the crystal and about 2.6 for the quasicrystals. The values are independent of the starting temperature of the sample.

The crossover from delayed to immediate plastic be-

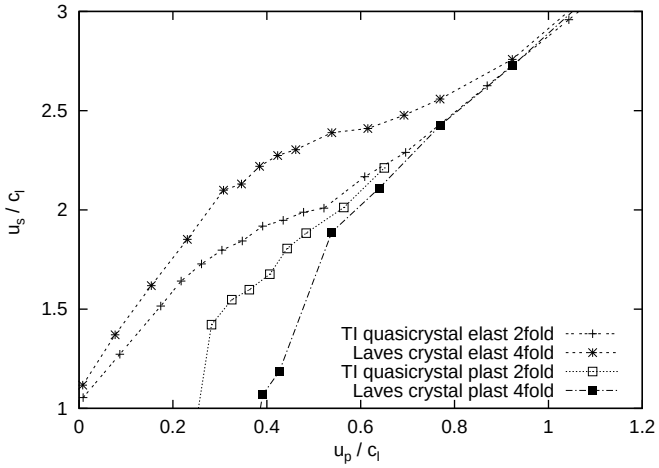

FIG. 5: Shock vs. piston velocity. At low piston velocity (quasi-)elastic behavior is observed. Between $u_p/c_l = 0.3$ and 0.6 approximately a crossover to the plastic shock wave and finally the change of slope to a materials-independent value is found. The velocities u_p and u_s are scaled by the velocity of sound c_l valid for the different directions.

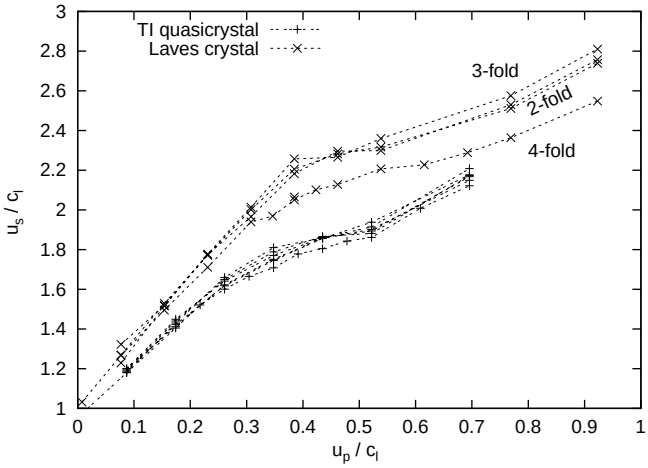

FIG. 6: Orientation dependence of the shock vs. piston velocities. The quasicrystal curves are identical if errors are taken into account. Therefore they are not marked individually. For the Laves crystal, the velocities along the 4-fold direction differ from the other orientations which on their part are again quite similar. The velocities u_p and u_s are scaled by the velocity of sound c_l valid for the different directions.

havior takes place between 0.3 and 0.6 u_p/c_l . The elastic front from the first regime is turned into an elastic precursor wave. Its height first decays slowly but it becomes steady during simulation. The elastic front is followed by a non-steady plastic precursor. The velocity given in Fig. 5 is not a shock front velocity, but the velocity of half height between the peak value of the shear pressure and its value at the center of the sample. This velocity is not half of the speed of the elastic wave, since the relaxation of the shear pressure is nonlinear across the sample. The half-height velocity is presented since it demonstrates how the sample switches from non-steady to steady behavior across the second regime.

At high piston velocities above, about $u_p/c_l = 0.6$, the material-independent plastic behavior occurs and *steady* shock waves are found. The elastic wave front is followed immediately by the plastic wave. In this regime the finite yield strength of the solids does not play a role any more.

In the whole range from $u_p/c_l = 0.2$ up to $u_p/c_l = 1.0$ at least, an additional *elastic* wave front is observed at the beginning of the simulation, moving with a velocity that has a constant slope $(u_s - c_l)/u_p = 3.1$ for the crystal and 2.6 for the quasicrystal, respectively, the same velocities as in the elastic regime (This wave is not shown in Fig. 5). It represents an elastic "one-dimensional" precursor wave. After a simulation time of $t = 0.05t_0$ the precursor wave vanishes and the ordinary elastic and plastic wave fronts take over. Obviously it takes a certain time interval until the coupling between the shock wave direction and the transversal directions becomes effective.

The Hugoniot curves obtained in the simulations do not depend on the sample cross-section and on the length of the rod as long as the shock wave has not penetrated the whole sample during simulation time and no interference with reflected waves has taken place.

In the crystal the crossover from elastic to plastic behavior occurs at shock wave intensities higher than in the quasicrystal. One reason may be that the local environment of a *single* atom is more symmetrical, while the opposite holds for the *averaged* environment. The transition to plastic behavior has to break the local symmetry to couple the normal and the transverse directions. The trigger are the random fluctuations induced by temperature, and the mechanism works better for lower site symmetry. A further reason will be presented in the section about the defects.

Usually there are sharp kinks in the Hugoniot plot between the different regimes if a phase transition occurs, with a flat gradient in the central part. The reason for the rather weak change of the slope in our case at about $u_p/c_l = 0.6$ may be on the one hand the difficulty to determine u_s accurately. But on the other hand there is no clear distinction between the second and third regime since we do not have an ordinary phase transition but a fragmentation of the sample with decreasing grains. The third regime is reached when the fragment size is of the order of a few interatomic distances. The reason why there is no kink between the first and second regime for the quasicrystals will be discussed in the section about the defects.

D. Orientation Dependence of the u_s-u_p Relation

Fig. 6 shows the Hugoniot plot for various propagation directions. In the TI-quasicrystals the curves along six different directions are all identical within the error bars if scaled with the velocity of sound for these directions. The result is a first hint that the plasticity modes are the same for all directions in the quasicrystal.

For the Laves crystal, the curves for shock waves propagating along the the 3-fold and 2-fold axes and in the direction perpendicular to a mirror plane are rather similar whereas a significant deviation exists for shock waves along the 4-fold direction. The difference between the curves in the second and third regime vanishes, however, if the velocities of the shock waves are scaled with the individual sound velocities. As in the case of quasicrystals, we conclude that there is no basic difference in the plasticity modes for the different shock propagation directions.

E. Analysis of Defects

Defects in quasicrystals are much harder to analyze than in ordinary crystals. In a crystal there is usually only a small number of different atom sites and a small number of neighborhoods. After a modification of the crystal it is easy to compare the status of an atom, for example its potential energy and the number of neighbors, to the allowed values in an ideal structure and to figure out which atoms belong to a defect. Such a procedure is not possible in a quasicrystal. Certainly, the environments of the atoms can be classified if only near neighbors are taken into account. In each class the atoms have another binding energy. But even in simple models like the ones considered here there exist of the order of 40 ideal environments which often differ very little from one another. Thus it is challenging to find out whether a change in the binding energy is due to a defective environment. To solve the problem we have tabulated the binding energy of each atom at the beginning of the simulation and compared the instantaneous binding energy to the stored value. Since the atoms vibrate around their equilibrium position and exchange kinetic and potential energy one has to introduce a temperature dependent tolerance interval for the binding energies. There are, however, still two possibilities if a change has occurred: the atom has jumped into another allowed neighborhood class, or it has become a defect atom.

Since shock waves generate large changes in energy, these classification methods do not work well for quasicrystals and also not for crystals. There is a second reason for the failure: the defects are not localized, but extended. We tried out several other indicators, but none worked well. The best we could find was a rescaling the sample after the shock wave has passed, in such a way that the distances between the initial and final position of the atoms were minimized. The minimization can easily be carried out qualitatively by trial and error if the displacement vectors are plotted as in Fig. 7. Then the scaling is varied until the vector lengths become as small as possible. A good overview of the defects is obtained if the shortest displacement vectors (or the longest) are removed and the remaining are plotted. The procedure permits us to extract vortices and thereby to map out the local rotation axis. A three-dimensional impression can be obtained by cutting slices and comparing them (See Fig. 7).

A second method which will work for any structure is to produce a list of nearest neighbor atoms in the initial structure. If a pair of atoms is in the list we say that the atoms are bound. By computing similar lists of atoms in the final states one can determine which bonds have been broken and if new bonds have been created.

A third procedure which turned out to be very helpful was to quench the sample after the shock. We discovered that it removes not only the kinetic energy and puts the atoms back into their local force-free state, but eliminates most of the local rotation of the sample (See Fig. 8).

F. Laves crystal

In this section we will discuss the results for the Laves crystal. Due to periodicity the results are much simpler to analyze than those of the quasicrystal.

The crystal structure remains perfect up to $u_p/c_l \approx 0.37$ which tells us that only elastic distortions occur in the first regime. Close to the shock front large displacements may be found, but these are transient phenomena.

Within a short interval of about $u_p/c_l = 0.1$ the behavior changes abruptly. Extended defects appear which separate perfectly crystalline domains. The defects start to fill up the bulk with increasing strength of the shock wave. Beyond $u_p/c_l \approx 0.57$ the initial structure seems to be destroyed completely by the shock wave. The size of the fragments into which the single crystal breaks become so small that the structure can no longer be distinguished visually from a disordered material. The radial distribution function, however, still contains a few discrete maxima since some small ordered regions are left over.

1. Defect Bands in Situ

A slice through the atomic displacement field represented in Fig. 7 illustrates the structure of the extended defects. Bands are visible with a width of up to 10 interatomic distances a and a separation of the order of $35a$. The bands are shear grain boundaries which separate different crystallites. It could be speculated that the bands are still molten, but such an assumption could not be confirmed by local temperature maps.

Within the crystallites rotation axes are observed. The edges and corners of the crystallites are given by hyper-

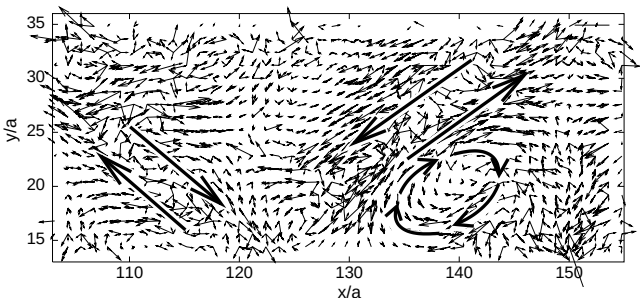

FIG. 7: In situ displacement field of the Laves crystal at $u_p/c_l = 0.45$. The large antiparallel arrows indicate slip planes. The ring of large arrows marks a rotation axis. Pictures of the quasicrystals look similar. The numbers at the figure represent the size in nearest neighbor distances a.

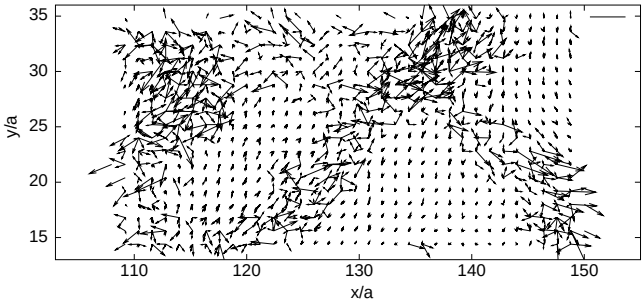

FIG. 8: Displacement field of the Laves crystal at $u_p/c_l = 0.45$ after quenching. Shown is nearly the same part of the sample as in Fig. 7. Pictures of the quasicrystals look similar. The numbers at the figure represent the size in nearest neighbor distances a.

bolic points (not visible in the figure). These are locations, where displacement vectors point towards one another along one direction while they point in opposite directions along a directions offset by 90 degrees. Thus the original mono-crystal is broken into crystallites which are deformed and rotated with respect to their initial orientation. If slices parallel to the coordinate directions are cut through the displacement field and compared we find that neither the grain boundaries nor the local rotation axis are perpendicular to the cutting direction. The local rotation axes turn out to be parallel to the face diagonals of the simulation box. Since the cuts through the grain boundaries are also parallel to the face diagonals we can conclude that the grain boundaries are perpendicular to the three-fold axes.

To our knowledge the rotation of crystallites in shock wave simulations on an atomic scale has not been reported before. Similar structures are well known from mesoscopic shock wave simulations by Yano and Horie[16,17] and by Makarov and co-workers[18–21] and discussed for example by Lee[22]. In the mesoscopic simulations the initial structure is already polycrystalline and phase boundaries exist, whereas in the simulations presented here we start with a single crystal which is broken into grains during simulation.

2. Defect Bands after Quenching

Fig. 8 shows the displacement field of the sample after quenching. The rotational part of the displacement field has disappeared, only the relative shift of the crystallites remains. The fragments can also be identified in a slice through the crystal (See Fig. 9). If the broken bonds are visualized we find that they mark the edges of the grains which look like more or less irregular polyhedral blocks. The final state of the quenched sample has been presented by Davison[23] as one of the states that occur if the deformation of the sample is not uniform.

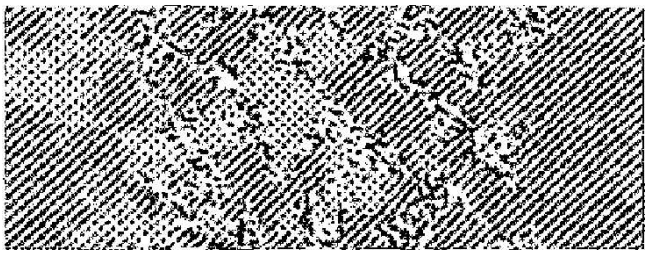

FIG. 9: Slice through the whole Laves crystal after quenching ($260 \times 61a^2$). The various textures (dotted and striped) are generated by displacements of parts of the sample with respect to each other and represent the newly created grains.

3. Summary of the Defects in Laves Crystals

The Laves single crystals are broken into grains by the shock wave in the second regime. The boundaries between the grains are broad disordered bands. The grains still contain the original Laves crystal structure, no phase transitions or twinning has been observed. The spacing between the bands depends on the cross section of the sample since the bands are replicated by the periodic boundary conditions. In the case of small cross sections the boundary conditions may even pretend a disordered state in the second regime. Stacking faults have not been observed and dislocations could not be detected.

If the shock wave intensity is increased, the general behavior of the Laves crystal does not change. The grains get smaller and smaller and the defect bands closer and closer until it is no longer possible to distinguish grains and bands. Then the third regime has been reached where the sample structure is destroyed completely.

G. Quasicystal Models

The Hugoniot curves for the quasicrystals look similar to those of the Laves crystal. A first glance at the

samples shows that the quasicrystals stay intact up to a piston velocity of about $u_p/c_l = 0.25$. But there is no sharp boundary between the (quasi-)elastic and the plastic regime (See Fig. 5). The reason will be discussed in the next paragraphs.

1. The TI-Quasicrystals

In the TI model ring processes, well known from equilibrium simulations[12], but enhanced by the shock wave are observed at very low shock wave intensity $u_p/c_l = 0.09$ already (Fig. 10). With increasing shock strength the rings break up and the atoms start to move around randomly (at $u_p/c_l = 0.17$). Well separated chains of atoms are now observed. At $u_p/c_l = 0.22$ it is no longer possible to speak of chains, we find clouds of atoms in motion. At $u_p/c_l = 0.26$ we finally have a situation similar to the Laves crystal: the sample is broken into crystallites which are shifted and rotated.

Thus we have two plasticity modes: the ring and chain processes which take place in the interior of the grains and the disruption of the single crystal into domains. This is the reason why there is no sharp boundary between the different shock wave regimes. In addition to the aperiodicity of the quasicrystal it is also the reason why it is so much harder to visualize the (quasi-)crystallites. The broken fragments are similar to those in the Laves crystals, but there shape is less polyhedral and the grains are smaller.

2. Behavior of the BI-Model

In the BI model the ring processes are suppressed completely since the configurations of tiles responsible for the jumps are removed. Only single atom flips are allowed. The displacement of the atoms at the shock front is large enough that some of them can jump to alternative sites where they remain after the shock wave has passed (Fig. 11). The jump locations can be considered as double-well potential sites. Since both positions are equivalent with respect to energy but separated by a barrier the atoms will not move back to their initial site.

Due to the point defects the transition from the elastic to the plastic regime is again much smoother in the BI-quasicrystals than in the Laves crystal. Since the number of jumps and the atoms involved are much less in the BI model than in the TI model the defects alone cannot be responsible for the weakness of the quasicrystals. Another reason has been pointed out in Sec. III C: Although the global symmetry of the icosahedral quasicrystals is higher than that of the cubic Laves crystals, locally many atoms in the quasicrystals have low symmetry whereas the atoms in the Laves crystal have a high central symmetry. We believe that this is the true reason why the threshold to generate defects is reduced considerably in the quasicrystal.

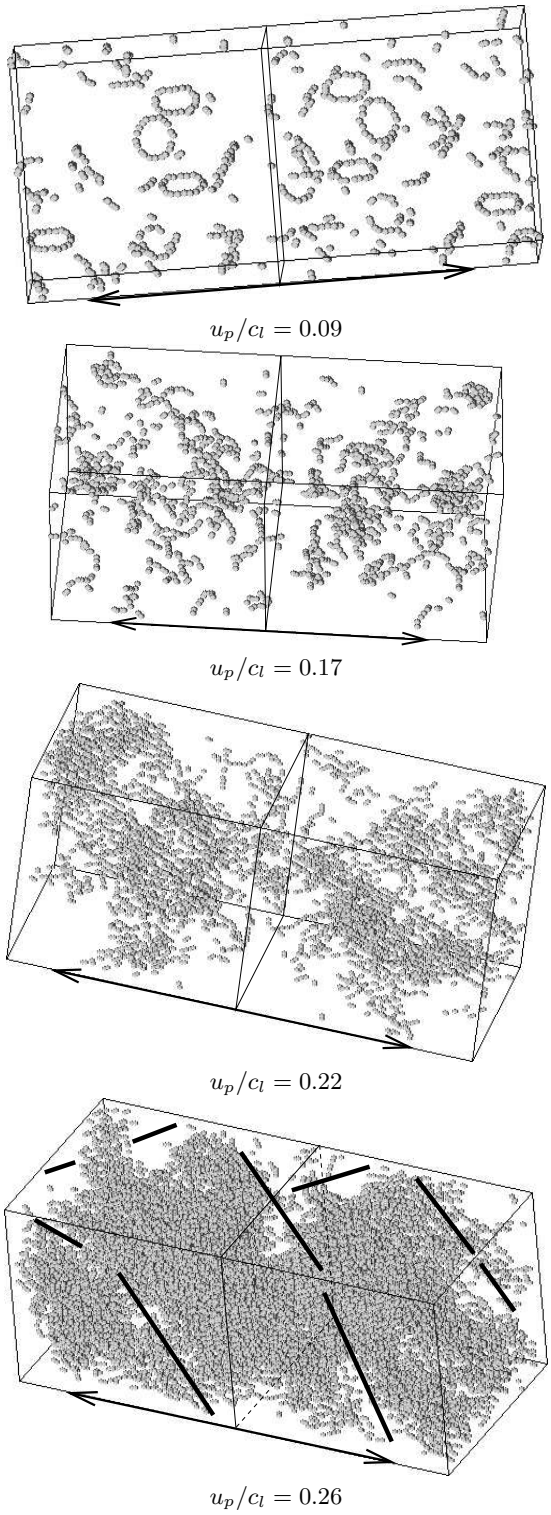

FIG. 10: Sequence of shocked samples of the TI-model. A third of the width and a fifth of the length has been cut out around the center of the simulation cell. The boxes are displayed to enhance the three-dimensional impression. The central squares show the starting place of the shock waves. The arrows indicate the path of the shock fronts which have left the boxes already at the recording time of the pictures. The thick black lines illustrate the local rotation axis. In the first two pictures the spheres represent the jumping atoms directly, while in the last two pictures they are overshadowed by clouds of atoms with large displacements.

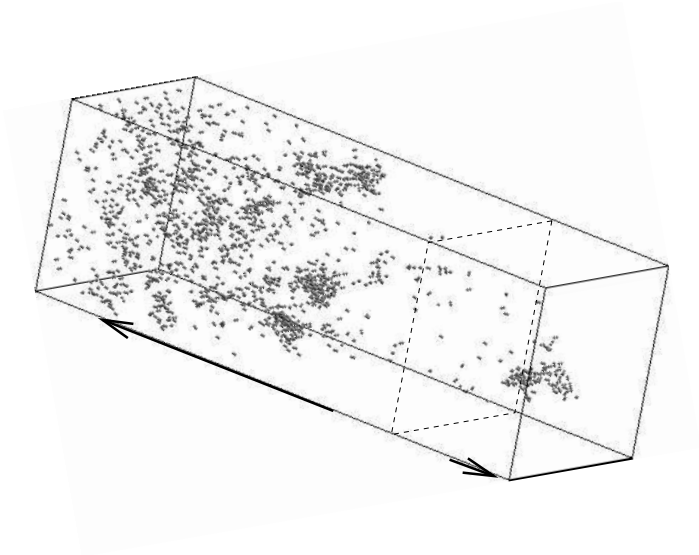

FIG. 11: Shock wave in the BI-model. Half the width and a third of the length has been cut out of the simulation cell. The box is displayed to enhance the three-dimensional impression. The square within the box represents the starting place of the shock waves and the arrows indicate the path of the shock fronts. In the instant represented in the picture the left-moving wave is at the left end of the box, whereas the right-moving wave has already left the box. The dots indicate atoms with large displacements. In the left half of the box many points disappear when the shock front proceeds further which emphasizes the transient character of the large displacements. Only a few singular points are left over like in the region where the shock waves started. They mark the sites where atoms have jumped to alternate positions.

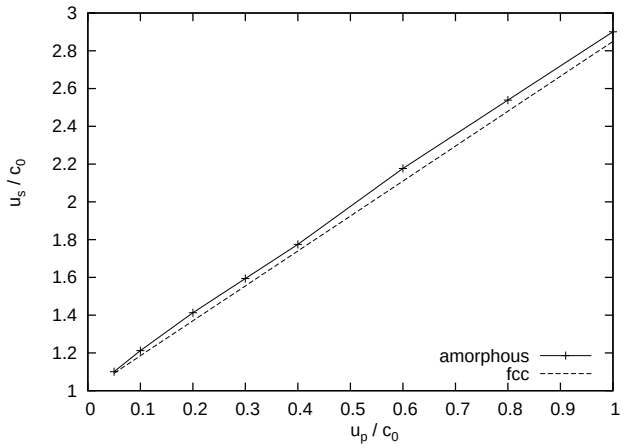

FIG. 12: Shock vs. piston velocity for the amorphous solid (dotted curve). The fcc curve (full line) is from Holian and Lomdahl[13].

3. *Summary of the Quasicrystal Results*

Between $u_p/c_l = 0.25$ and 0.5 extended defects can be observed in both quasicrystal models. A process similar to the one in the Laves crystals takes place: the grains get smaller and smaller and the defect bands move closer and closer together. At shock waves stronger than $u_p/c_l = 0.5$ the quasicrystals appears disordered since defect bands and grains can no longer be distinguished.

Again we find no stacking faults and no dislocations. Quasicrystal-specific defects like phason walls have not been observed as well. Although we have seen atoms jump, we know[12] that these processes are *no* quasicrystal flips since the jumps do not change the rhombohedron-dodecahedron tiling. Real flips are very complicated in the quasicrystal models presented here and involve at least 10 atoms.

H. Amorphous Solid

In the case of the amorphous solid we find a universal behavior for all shock front velocities: The slope of the Hugoniot curve is $u_s/c_0 = 1.85 \cdot u_p/c_0 + 1.0$ up to $u_p/c_0 = 1.0$ (See Fig. 12). This is no indication, however, that the amorphous structure behaves like a fluid. If we consider the pressure profiles, especially the shear pressure, we find that up to $u_p/c_0 = 0.2$ the profiles are unsteady as a whole. There is a steady jump from the elastic compression wave followed by an slow decay which lasts the whole length of the sample. At $u_p/c_0 = 0.3$ we find a transitional behavior, but at $u_p/c_0 = 0.4$ we clearly observe steady waves. The shear pressure decays within a short interval to a finite constant value. If we compare this behavior to Fig. 5 we find that the transition to the steadiness of the plastic waves occurs at approximately the same shock strength as in the ordered samples. It also indicates that the amorphous solid possesses a finite yield strength since the shear pressure is not zero.

The amorphous solid stays disordered. No obvious change of the structure has been notified by inspection of the radial distribution function for example. In particular, crystallization has also not been observed.

IV. DISCUSSION

Our study has revealed yet another type of plasticity observable in atomistic simulations beyond simple dislocations and stacking faults[13] and phase transitions[1,3,24]. Here we find fragmentation of a single crystal into rotated crystallites separated by thick disordered walls.

The behavior of the crystal and the quasicrystal models in shock wave simulations is similar to the behavior of ionic materials: slippage is hindered by the creation of high-energy anti-phase boundaries. Dislocations are slow, rare and high energies are needed to generate them[25]. The single-crystal ionic materials break into many crystallites and form broad defect bands[26]. In the models presented here it is not possible to exchange A

and B atoms at random without destabilizing the structure. If an AB bond is broken it will be replaced by an AA or BB bond which is only half as strong. Due to the nontrivial plane structure it may also happen that no new bond is formed. Furthermore the structure will be strained, since the different bonds are of different length. The average binding energy decreases. Thus processes allowed in monatomic structures turn out to be fatal. Recent crack simulations have shown that the Laves phase and the quasicrystal always behave brittle[27]. No dislocation emission could be observed.

But on the other hand it is well known that stacking faults exist in Laves crystals and a synchroshear mechanism[28] which should permit slippage. Since our models are stable in a large range of interaction strengths, it would be interesting to repeat the simulations with a parameter set where the repulsion is reduced. But calculations of the γ-surface? for a number of parameter sets by C. Rudhart[29] dash the hope. Although the heights of the energy minima and maxima might vary, the overall topology of the surface stays largely the same. No shift vectors exist which would indicate low energy dislocation directions.

We have found that there is a material-independent Hugoniot relation governed by the interaction only in the case of strong shock waves. This is due to the complete destruction or amorphization of the structures, a phenomenon which is well known from high-pressure studies of C15 Laves phases.

We have tried to find crystal and quasicrystal structures which are as similar as possible. The best model would be monatomic, but no uniform simple monatomic quasicrystals exist (But see Roth[24]). There are still differences in the average binding energies, the composition, and the local atomic environments in our models. Therefore we cannot rule out that part of the results (for example the different slopes in the Hugoniot plot) are due to the structural differences.

Defect structures and plasticity modes have been presented for propagation directions of the shock waves along the four-fold direction in the Laves crystal which is oblique to the close-packed planes, and along the two-fold direction in the quasicrystal which is normal to the close-packed planes. Although these two directions are quite different with respect to the orientation of the prolate rhombohedra, the results are rather similar. Simulations in other symmetry directions have also been carried out, but they have not been discussed since no new phenomena have been observed. We consider this observation as a further indication that the phenomenology of the shock wave plasticity in the present study is governed mainly by the interaction and not by the structure.

Up to now no shock wave experiments have been carried out with quasicrystalline materials. There are a number of high-pressure studies which demonstrate the high strength of quasicrystals[30]. But the high-pressure studies do not lead to the high temperatures typical for shock waves. It has been found that quasicrystals are often transformed into approximants under high pressure, but such a transition has not been observed in our simulations.

The behavior of Laves crystals under high pressure is well-studied (See for example Lindbaum et al.[31]). The crystals are preferably amorphized similar to what happens if they are heavily loaded with hydrogen. Shock-wave experiments of Laves phases have not been found in the literature, especially no reports are known to us about the investigation of defect structures caused by shock waves. Frank-Kasper-type quasicrystals like AlCuLi behave similar to the Laves crystal, except that crystallization is also observed[32].

Acknowledgments

I am especially indebted to Ralf Mikulla who has pointed out to me a number of problems in earlier shock wave simulations and has supplied me with valuable references. Helpful discussions with Kai Kadau, Christoph Rudhart and Hans-Rainer Trebin are also acknowledged.

[1] T. C. Germann, B. L. Holian, P. S. Lomdahl, R. Ravelo, Phys. Rev. Lett. **84**, 5351 (2000).
[2] J.-B. Maillet, M. Mareschal, L. Soulard, R. Ravelo, P. S. Lomdahl, T. C. Germann, and B. L. Holian, Phys. Rev. E **63**, 016121 (2001).
[3] K. Kadau, T. C. Germann, P. S. Lomdahl, and B. L. Holian, Science **296**, 1681 (2002).
[4] D. Tanguy, M. Mareschal, P. S. Lomdahl, T. C. Germann, B. L. Holian, and R. Ravelo, Phys. Rev. B **68**, 144111 (2003).
[5] B. L. Holian, Shock Waves, **5**, 149 (1995).
[6] J. Roth, in *Proc. of the Workshop on Molecular Dynamics on Parallel Computers*, edited by R. Esser et al., (World Scientific Singapore, 1999), p 83.
[7] J. Roth, Mat. Sci. Eng. A **294-296**, 753 (2000).
[8] J. Roth, Ferroelectrics **250**, 365 (2001).
[9] P. Kramer, R. Neri, Acta Cryst. A. **38**, 257 (1982).
[10] J. Roth, R. Schilling, and H.-R. Trebin, Phys. Rev. B **41**, 2735 (1990).
[11] C. L. Henley and V. Elser, Phil.Mag. **B53** L59 (1986).
[12] J. Roth, Euro. Phys. J. B **15** 7 (2000).
[13] B. L. Holian, and P. S. Lomdahl, Science **280** 2085 (1998).
[14] IMD stands for **I**TAP **m**olecular **d**ynamics. J. Stadler, R. Mikulla, and H.-R. Trebin, Int. J. Mod. Phys. C **8** 1131 (1997); J. Roth, F. Gähler, and H.-R. Trebin, Int. J. Mod. Phys. C **11**, 317 (1997). The home page of IMD can be found at www.itap.physik.uni-stuttgart.de/~imd.
[15] D. C. Wallace, Phys. Rev. B **22**, 1487 (1980).
[16] K. Yano, Y. Horie, Phys. Rev. B **59**, 13672 (1999).

[17] K. Yano, Y. Horie, Int. J. Plast. **18**, 1427 (2002).
[18] R. R. Balokhonov, P. A. Makarov, V. A. Romanova, I. Yu. Smolin, Comp. Mat. Sci. **16**, 355 (1999).
[19] I. Yu. Smolin, P. A. Makarov, D. V. Shmick, I. V. Savlevich, Comp. Mat. Sci. **19**, 133 (2000).
[20] P. V. Makarov, V. A. Romanova, Theo. Appl. Frac. Mech. **33**, 1 (2000).
[21] P. V. Makarov, Theo. Appl. Frac. Mech. **33** 23 (2000).
[22] J. Lee, in *High-Pressure Shock Compression of Solids VI*, edited by Y. Horie, L. Davison, and N. N. Thadhani, (Springer New York, 2002), chap. 2, p 121.
[23] L. Davison, in *High-Pressure Shock Compression of Solids VI*, edited by Y. Horie, L. Davison, and N. N. Thadhani, (Springer New York, 2002), chap. 1, p 16.
[24] J. Roth, submitted to Phys. Rev. B.
[25] G. Schaaf, J. Roth, and H.-R. Trebin, Phil. Mag. **83**, 2449 (2003).
[26] T. Mashimo, in *High-Pressure Shock Compression of Solids III*, edited by L. Davison and M. Shahinpoor, (Springer Heidelberg, 1998), chap. 5, pp 101-146.
[27] F. Rösch, C. Rudhart, H.-R. Trebin, P. Gumbsch, submitted to Phys. Rev. Lett.
[28] P. M. Hazzledine, K. S. Kumar, D. B. Miracle, A. G. Jackson, Mat. Res. Soc. Symp. **288**, 591 (1993).
[29] C. Rudhart, private communication.
[30] H. M. Kimura, K. Sasamori, and A. Inoue, Mat. Sci. Eng. A **294-296**, 168 (2000).
[31] A. Lindbaum, E. Gratz, and S. Heathman, Phys. Rev. B **65**, 134114 (2002).
[32] Y. Akahama, Y. Mori, M. Kobayashi, H. Kawamura, K. Kimura, and S. Takeuchi, in Proc. of the XIII AIRAPT conf. Recent Trends in high pressure research, p. 156 (1991), Y. Mori, Y. Akahama, M. Kobayashi, H. Kawamura, K. Hamada, and M. Motoyama, J. Phys. Soc. Jpn **58**, 1482, 2231 (1989).

TI stands for truncated icosahedra, also known as Bergman clusters, a prominent structural feature of the model.
BI denotes binary icosahedral (model), also known as Henley-Elser model.
Reduced units are used throughout the paper. Lengths are given in a, and energies in ϵ. All other units are converted into a, ϵ and the mass m. Thus we have $t_0 = a\sqrt{m/\epsilon}$, $v_0 = \sqrt{\epsilon/m}$, and $P_0 = \epsilon/a^3$
The γ-surface represents the increase in energy with respect to a displacement vector if a sample is cut into two parts which are shifted laterally with respect to each other by this vector.